cent study of Ref. 3, the results of which are also within 1% of Eq. (1). Thus, Eqs. (1) and (2) are expected to provide an accurate determination of $\dot{q}$ from thin-film gages on MACOR substrates, which, in turn, allows detailed heating distributions to be measured accurately on complex models in conventional hypersonic wind tunnels that are not possible with transient calorimeter techniques, as demonstrated in Ref. 3.

Because of the small size of the hemispheres, corresponding to relatively low values of Reynolds number based on nose radius, the present results also provide information on viscous effects on stagnation-point heating. As the Reynolds number is reduced, classical boundary-layer theories (see, for example, Ref. 5), initially underestimate heating as viscous effects become significant, then progressively overestimate heating as slip effects become significant. This trend is well documented in the literature and is illustrated by the curves in Fig. 2 which were taken from Ref. 6. Each of the five hemispheres revealed an effect of Reynolds number on stagnation-point heating in the Mach 10 Tunnel, with $C_h/(p_{t,2}/r_n)^{1/2}$ increasing about 8% as R_{∞,r_n} decreased from 32.5 to 7.9×10^3. Viscous effects were also evident in the comparison of measured heating for the quartz hemispheres to that predicted by the theory of Fay-Riddell.[5] This comparison is shown in Fig. 2 where the ratio of measured-to-predicted stagnation-point heating is plotted as a function of the post-shock Reynolds number and the normal shock density ratio. Now, since the thin-film element covers the stagnation region within 10 deg of the stagnation point, the measured heating rate will be lower than the stagnation-point value by 1-2%. Possible vibrational nonequilibrium effects may also tend to lower the heating. Nevertheless, viscous effects are observed in Fig. 2 to cause the measured heating to exceed classical boundary-layer prediction by up to 10% for the present Mach 10 flow conditions in air. Measured heating rates in Mach 10 air also exceeded values predicted with a code[7] that solves the Navier-Stokes equations but by no more than 5% (experimental uncertainty). Measured heating rates in Mach 6.4 CF_4 presented in Fig. 2 are nondimensionalized by values predicted using a boundary-layer code and the thermodynamic properties for CF_4 given in Ref. 8. These CF_4 results are of particular interest since they simulate the increase in shock strength that occurs for a blunt body during reentry due to dissociation within the shock layer. The experimental results of Fig. 2 show the influence of viscous effects on heating increases substantially with increasing shock strength for the present range of Reynolds number, in agreement with the predictions of Ref. 6.

References

[1]Miller, C. G., "Comparison of Thin-Film Resistance Heat-Transfer Gages with Thin-Skin Transient Calorimeter Gages in Conventional Hypersonic Wind Tunnels," NASA TM 83197, Dec. 1981.

[2]Schultz, D. L. and Jones, T. V., "Heat-Transfer Measurements in Short-Duration Hypersonic Facilities," AGARD-AG-165, Feb. 1973.

[3]Wannenwetsch, G. D., Ticatch, L. A., Kidd, C. T., and Arterbury, R. L., "Results of Wind Tunnel Tests Utilizing the Thin-Film Technique to Measure Wing Leading-Edge Heating Rates," AEDC-TR-83-50, May 1984.

[4]Miller, C. G., "Measured Pressure Distributions, Aerodynamic Coefficients, and Shock Shapes on Blunt Bodies at Incidence in Hypersonic Air and CF_4," NASA TM 84489, Sept. 1982.

[5]Fay, J. A. and Riddell, F. R., "Theory of Stagnation Point Heat Transfer in Dissociated Air," *Journal of Aeronautical Sciences*, Vol. 25, Feb. 1958, pp. 73-85, 121.

[6]Gilbert, L. M. and Goldberg, L., "A Reynolds Number Scaling Theory for Hypersonic Ablation," AIAA Paper 67-155, Jan. 1967.

[7]Gnoffo, P. A., "A Vectorized, Finite-Volume, Adaptive Grid Algorithm Applied to Planetary Entry Problems," AIAA Paper 82-1018, June 1982.

[8]Sutton, K., "Relations for the Thermodynamic and Transport Properties in the Testing Environment of the Langley Hypersonic CF_4 Tunnel," NASA TM 83220, Oct. 1981.

[9]Wittliff, C. E., private communication, Calspan Advanced Technology Center, Buffalo, N.Y.

An Adaptive Finite Element Technique for Plate Structures

M. E. Botkin*
General Motors Research Laboratories
Warren, Michigan

Introduction

THERE have been several papers written on the subject of adaptive mesh generation;[1-3] however, few have emphasized the complete model building process.[4] The emphasis in Refs. 1-3 tends to be the determination of the solution quantity used as a refinement criterion, but such systems do not automatically obtain an initial mesh or carry out the refinement process. The process described by Shephard[4] addresses the abovementioned features, but relies heavily on interactive graphics to tailor the refined mesh. It was desired to develop a technique that could be used with shape optimization,[5] as well as to have an efficient modeling technique that relieves the analyst of much of the work of finite element modeling. For this reason, three major features were required: 1) mesh refinement based upon an initial solution, 2) efficient modeling of the initial mesh, and 3) "blackbox" operation.

Structural components subject to bending deformations are of particular interest to the automotive industry. None of the authors of mesh refinement papers have treated bending problems, probably due to the undesirable characteristics of bending-type finite elements. An example with bending has been included in this Note.

Mesh Refinement

The mesh refinement process is based upon the variation in strain energy density (SED) as a measure of the error in an element. In order to show this, consider the relationship[4] expressing the error in a solution quantity in an element in terms of the variation in that quantity

$$|V-V_I|_e \le C_j h_e^k |D^k V|_e \tag{1}$$

where V is some exact solution quantity (stress or SED), V_I the computed value, C_j a proportionality factor, h_e the element size, and D^k a differential operator of order k (the order of the element). For constant-strain elements ($k=1$), the error is proportional to the element size times the first variation in the solution quantity. The following empirical relationship has been proposed in Ref. 4 for determining a level of SED variation above which the elements will be subdivided:

$$CV=\overline{\Delta E}+\beta(\Delta E_{\max}-\overline{\Delta E}) \tag{2}$$

in which CV is the SED difference cutoff value, $\overline{\Delta E}$ the average SED variation for all elements, $\Delta E_{\max}$ the maximum SED variation in any element, and β a parameter to be selected based upon the problem but generally lying between 0 and ½.

Obviously, the accuracy due to any refinement is unknown in advance. Although numerous papers have been written on error estimates of total strain energy (many of which have been noted in Ref. 6), this work cannot be readily extended to stresses and displacements. For the case of shape optimization, it is desired to have a conservative estimate of the converged finite element solution. This information may be obtained using a linear extrapolation technique, such as graphically represented by Fig. 1. This is a typical relationship

Received Oct. 6, 1983; revision received June 21, 1984.

*Staff Research Engineer, Engineering Mechanics Department.

between a solution quantity and the mesh size. Several steps of refinement are shown, with each step having reduced the element size in half. The solution will eventually converge (S_e) and the slope of the curve reflects the rate of convergence. For stresses, the slope can be quite large due to the local nature of the refinement. For displacements, the slope may not be great but, in general, the overall accuracy is better. A conservative estimate of the converged solution, represented by points S_i^0 or S_i^1, may generally be obtained by extrapolating the data points produced by one unrefined analysis and a single refined analysis. It has been found that this technique is more reliable for the plane stress element than for the bending element due to the slightly nonconforming qualities of that element. Finally, it should be noted that Fig. 1 is not valid and the described technique will not work for the case of a stress at a singularity for the elements used here.

Applications

The technique described in this paper will be demonstrated on both bending and stretching examples in which the solutions have been obtained from the literature. All of the connectivities have been established using an automatic triangulation technique described in Ref. 7.

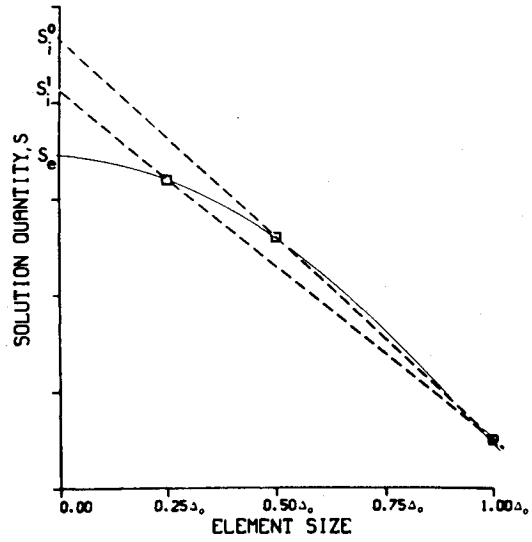

Fig. 1 Typical solution convergence.

Circular Hole in an Infinitely Long Plate

Figure 2a shows a finite element model for a uniformly loaded, plane rectangular plate. Due to symmetry, one-fourth of the plate is modeled. The entire plate is 1.524 m (60 in.) long and 0.508 m (20 in.) wide, with a 0.0508 m (2 in.) radius hole. A uniform load of 0.175 kN/m (1 lb/in.) is applied to the ends of the plate. The uniform thickness is 0.0254 m (1 in.). The maximum stress occurs at point A of Fig. 2a and its value can be found in Ref. 8 to be 0.0216 MPa (3.135 psi). It should be noted that, due to the finite plate width, this value differs from the classic case of a hole in an infinite plate in which the maximum stress would be 0.0195 MPa (3 psi). Three refined solutions were obtained using different initial mesh sizes, as shown in Fig. 2d. The maximum stresses appear to be converging to the theoretical value. The extrapolated stress estimates are represented by the straight lines passed through each unrefined-refined pair, and the error in these values varies between 3.8 and 5.4% on the conservative side.

Simply Supported Cylindrical Shell[9]

The cylindrical shell shown in Fig. 3a was chosen as an example that includes both bending and membrane deformations. The shell is supported at its ends by a rigid diaphragm and is loaded by its own weight. Only one-fourth of the shell was modeled and the initial finite element mesh is shown in Fig. 3a. Two initial mesh sizes were analyzed using three-noded finite elements that included combined bending and stretching deformations. Two levels of mesh refinement were used in which the highest level produced one-fourth of the initial element size Δ_0. The SED variation contours are shown in Fig. 3c and a typical refined mesh is shown in Fig. 3d. The maximum stress was found to occur at point A of Fig. 3a and to have a magnitude of 11.919 MPa (249,110 psf). Several initial mesh sizes were used and the refined analysis results are shown in Fig. 3e. The refined results tend to converge to the theoretical stress, but with some scatter in the data. The estimate for the converged stress in this case was 1.6% in error. Due to the scatter in the data, this is probably fortuitous. However, the range of estimates for all of the refinements was 5.1-1.6% in error, which is felt to be acceptable.

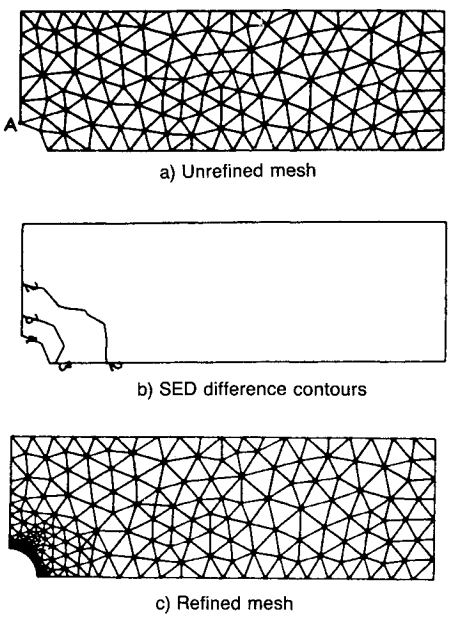

Fig. 2 Plate in tension with circular hole.

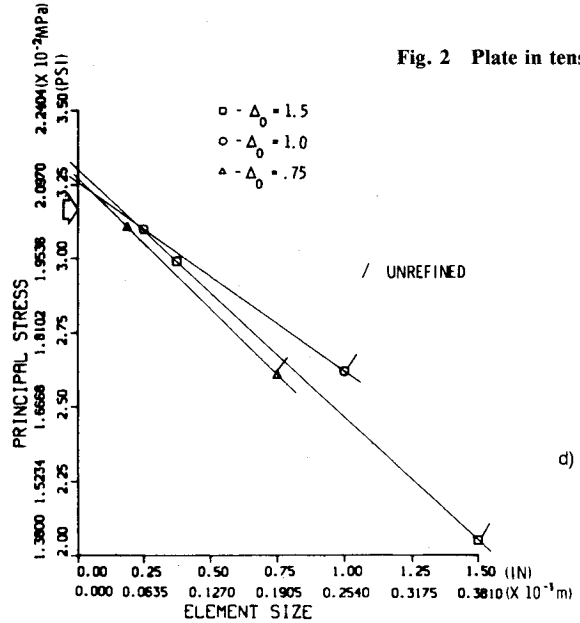

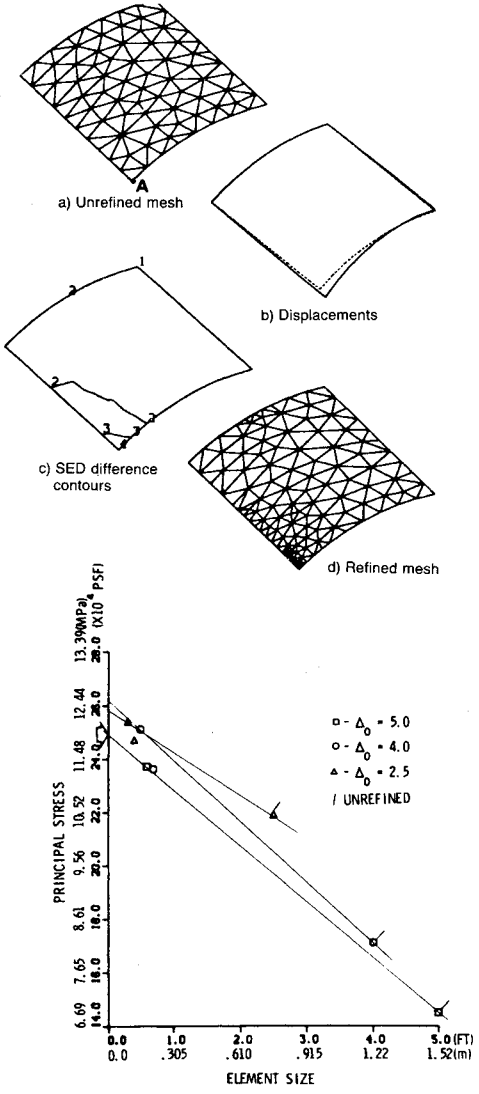

Fig. 3 Cylindrical shell with uniform gravity load.

Summary and Conclusions

An adaptive finite element technique has been described that can be used to analyze plate-like structural components with combined bending and stretching deformations. High variation in the strain energy density within an element is the measure used as the refinement criterion. Emphasis is placed upon the overall analysis model generation process, which is composed of an initial, uniform mesh followed by an automatically refined mesh. An important feature of the method is the ability to obtain high-quality results with only a single refinement. A simplified, linear extrapolation technique is used to estimate the converged solution. The method was applied to examples for which exact solutions were available from the literature, and was found to yield high-quality results of generally less than 5% error (for stresses).

References

[1]Turke, D. J. and McNeice, G. M., "Guidelines for Selecting Finite Element Grids Based on an Optimization Study," *Computers and Structures*, Vol. 14,, Oct. 1973, pp. 499-519.

[2]Melosh, R. J. and Marcal, P. V., "An Energy Basis for Mesh Refinement of Structural Continua," *International Journal for Numerical Methods in Engineering*, Vol. 11, 1977, pp. 1083-1091.

[3]Carroll, W. E., "On the Reformation of the Finite Element Method," *Computers and Structures*, Vol. 8, 1978, pp. 547-552.

[4]Shephard, M. S., "Finite Element Grid Optimization with Interactive Computer Graphics," Ph.D. Thesis, Dept. of Structural Engineering, Cornell University, Ithaca, N.Y., 1979.

[5]Bennett, J. A. and Botkin, M. E., "Shape Optimization with Geometric Description and Adaptive Mesh Refinement," *AIAA Journal*, Vol. 23, March 1985, pp. 458-464.

[6]Babuska, I. and Rheinboldt, W. D., "Adaptive Approaches and Reliability Estimations in Finite Element Analysis," *Computer Methods in Applied Mechanics and Engineering*, No. 17/18, 1979, pp. 519-540.

[7]Cavendish, J. C., "Automatic Triangulation of Arbitrary Planar Domains for the Finite Element Method," *International Journal of Numerical Methods in Engineering*, Vol. 8, 1974, pp. 679-695.

[8]Flynn, P. D., "Photoelastic Comparison of Stress Concentrations Due to Semicircular Grooves and a Circular Hole in a Tension Bar," *ASME Journal of Applied Mechanics*, Vol. 36, Dec. 1969, pp. 892, 893.

[9]Scordelis, A. C. and Lo, K. S., "Computer Analysis of Cylindrical Shells," *Journal of the American Concrete Institute,* Vol. 61, May 1964, pp. 539-561.